A Parameterization of the Particle Size Spectrum of Ice Clouds in Terms of the Ambient Temperature and the Ice Water Content[1]

ANDREW J. HEYMSFIELD

National Center for Atmospheric Research,[2] Boulder, CO 80307

C. M. R. PLATT

CSIRO Division of Atmospheric Research, Aspendale 3195, Australia

(Manuscript received 22 August 1983, in final form 29 November 1983)

ABSTRACT

A data set obtained in cirrus clouds has been examined to deduce any dependencies of the particle size spectral form or the crystal habit on the temperature. It was found that both form of the spectra and crystal habit changed systematically with temperature, the largest change occurring between −40 and −50°C. These findings are consistent with previously found dependencies between lidar backscatter measurements and temperature.

A preliminary scheme for parameterizing the cirrus particle size spectra for crystal dimensions greater than 20 μm in terms of the temperature and the ice water content is described. The visible extinction in cirrus is estimated.

1. Introduction

The World Climate Program has identified cloudiness and radiation as one of the main priority areas for climate research. At present, only rudimentary methods are used for including clouds in climate models, although some progress has been made in this area recently. Even if clouds can be predicted realistically in models, there is then the problem of predicting the cloud optical properties; it is the magnitudes of the cloud albedo and the infrared emittance, as well as the cloud altitude and temperature, which determine how the cloud will affect the radiation divergence in the atmosphere and the net global radiation at the top of the atmosphere and at the surface. Stephens and Webster (1981) and Platt (1981) have demonstrated the extreme sensitivity of the net global radiation to the optical depth of high cloud, or cirrus. It is recognized that it is unlikely that a global numerical model could ever contain sufficient detail to predict the particle size spectrum in a cloud, even if it was known how to do this. The most that is likely to be predicted is the cloud height, depth and the liquid or ice water content. Thus, ways of parameterizing the cloud optical properties in terms of the liquid or ice water content are necessary for progress. It has been shown (Paltridge, 1974; Platt, 1976; Stephens, 1978; Chylek, 1978; Chylek and Ramaswamy, 1982) that a parameterization of infrared radiation is possible for water clouds whose particle size spectrum peaks at a radius of about 5 μm—i.e., for stratocumulus, stratus and fair weather cumulus. The reason that these cloud properties can be parameterized in terms of the cloud liquid water content in the infrared is that the infrared extinction efficiency (extinction cross-section/geometrical cross-section) increases almost linearly with particle radius (r) for wavelengths in the 8 to 13 μm region of the optical spectrum where most of the radiation exchange takes place between boundary layer clouds and space. For a given liquid water content, the particle geometrical cross-section decreases as $1/r$. Thus, for a given liquid water content, the extinction cross-section is effectively independent of particle radius.

The same parameterization does not hold for ice clouds where the particle size tends to be larger than the wavelength. The infrared extinction efficiency then approaches unity and the extinction cross-section (and thus cloud optical depth) varies as $1/r$.

The motivation for the present work arose out of a lidar and radiometer study on cirrus clouds (Platt and Dilley, 1981, hereafter PD). What the study indicated was that a sudden change in the backscatter characteristics of cirrus cloud particles occurred between temperatures of −28 and −45°C. Fig. 1, which is taken from PD, shows the quantity $k/(2\eta)$ plotted against cloud temperature, as measured by lidar, and averaged over many cloud systems. Here k is the effective backscatter to extinction ratio of the cloud particles and as

[1] This work represents an equal contribution by both authors.

[2] The National Center for Atmospheric Research is sponsored by the National Science Foundation.

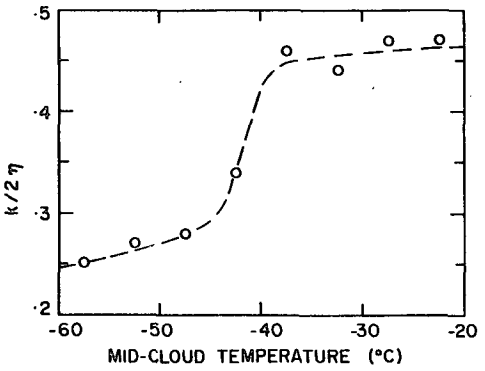

FIG. 1. The temperature dependence of the lidar-measured backscatter to extinction ratio $k/2\eta$; η is a multiple scattering factor ~ 0.5 (after Platt and Dilley, 1981).

$\eta \approx 0.5$, the curve approximates the behaviour of the former quantity; k is also numerically equal to the normalized scattering phase function in the 180° direction, a quantity which is related directly to the fundamental scattering properties of the cloud particles. Thus changes in k with temperature would signify corresponding changes in either the cloud particle phase, the ice crystal habit or the particle size concentration spectrum with temperature. Such systematic changes in these quantities might point to a method of their parameterization in terms of cloud temperature and thus, a parameterization of the cloud optical properties, albedo and emittance.

As it happened, a body of data on the particle size spectra and crystal habits in cirrus clouds at various temperatures already existed (Heymsfield, 1977) and for clouds similar in structure to those used in the PD study. Thus it was decided to analyze the variation of the shapes of these size spectra and the corresponding crystal habits to identify any systematic changes with temperature for either parameter. The data were also examined to decide whether it was indeed possible to represent the cirrus particle size distributions through a simple parameterization scheme.

2. The cirrus particle data

The data set was collected during the period 1973–75 with meteorological aircraft. Details of the meteorological situations and aircraft instrumentation are given in Heymsfield (1977). Most studies were made aboard a Cessna Citation jet. Sampling was carried out in relatively uniform and deep winter and springtime ice clouds associated generally with synoptic depressions. The aircraft sampling patterns were selected to collect representative data on the vertical distribution of the cloud particles. Each sampling pass was parallel to the wind and about 25 km in length. Most aircraft sampling profiles consisted of successive steps in 600 m increments down from the cloud top, which typically ranged between 8.5 and 11 km, to cloud base.

Three Particle Measuring System (PMS) probes were carried aboard the aircraft: a forward scattering spectrometer probe (FSSP) sizing in the range 2 to 30 μm in 2 μm intervals, a one-dimensional (1D) optical array probe (1D-C) sizing in the range 20–300 μm in 20 μm intervals, and a 1D probe ("1D-P") sizing in the range 200–3000 μm in 200 μm intervals. The data collected in each size channel were averaged over an entire pass to calculate "pass-averaged" concentrations. As discussed in Appendix A, some of the reduced data was of questionable accuracy; therefore, only those portions of the data set which seemed to be fairly reliable were used in these analyses. Other aircraft instrumentation included devices for measuring the state parameters and a continuous Formvar replicator, providing data for identifying the particle habits; problems with the identification of crystals of sizes larger than about 200 μm were noted because of crystal break-up upon impact on the replicator (see Appendix A). As virtually no droplets were noted in the replicator data with sizes larger than about 15 μm, all particles sampled with the 1D-C and 1D-P probes were considered to be ice crystals.

From the particle spectra data and the data on the nature of the crystal habits, Heymsfield (1977) estimated the ice water content (*IWC*) corresponding to each pass-averaged concentration.

The data used in the present study are those obtained in clouds with bases exceeding 3 km MSL and base temperatures below about −20°C (see Table 1). (The aim was to include only those cloud systems sampled in the Heymsfield study which had no visual precipitation reaching the surface and which had temperatures comparable to those in the clouds investigated by PD). The pass-averaged cirrus particle size spectra were grouped into 5°C temperature increments from −20 to −60°C. As indicated in Table 2, column B, the number of sampling passes within each 5°C temperature interval was small; thus, only some basic features of the dependence of the cirrus particle size spectra on the temperature might be expected.

3. Results of the data analysis

a. Particle size spectra

Changes in the basic features of particle size spectra over the temperature range −20 to −60°C were examined by averaging all spectra within each 5°C temperature interval. The resultant temperature-averaged size spectra are indicated in Figs. 2 and 3 in terms of the measured particle dimension and for dimensions greater than 20 μm. For reasons given in Appendix A the 2–20 μm FSSP data were excluded from the analysis. The dimensions represent the maximum crystal dimensions since corrections were made to account for undersizing of the non-spherical (columnar) crystals

TABLE 1. Summary of measurements.

Flight number	Synoptic indication	Sampling altitudes (km)	Temperature range (°C)
P2	Jet stream band	7–8.3	−27 → −35.4
P3	Overrunning with jet	6.9–9.1	−20.7 → −38.5
P4	Overrunning with jet	7.6–10.6	−27.9 → −52.9
P5	Overrunning with jet	4.6–10.6	−21.9 → −52.9
P6	Overrunning with jet	3.2–9.9	−15.4 → −60.3
P10	Post occlusion with strong jet	7.7–9.15	−35.4 → −47.8
P11	Overrunning with jet	10.5–11.2	−55.3 → −55.7
P12	Overrunning with jet	8–10.7	−33.2 → −49.6

(Heymsfield, 1977). The extent to which the particle concentrations varied amongst the individual spectra in each temperature interval are discussed later. The cloud *IWC*s were also averaged for each temperature interval. These averages are shown as *IWC* in column E of Table 2 and include the FSSP data as well, that is, they represent the total *IWC* of the cloud. Allowing for uncertainties in the FSSP spectra, the ice contents are estimated to be accurate to within 20%. They are

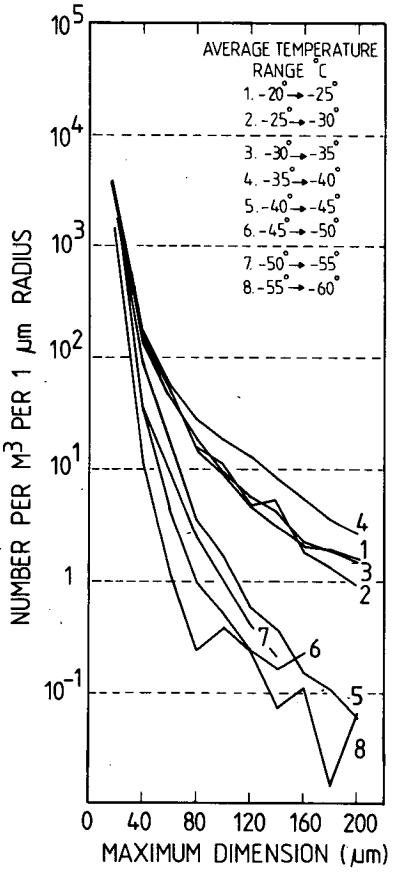

FIG. 2. Average particle spectra in different temperature ranges for the 20–300 μm crystal maximum dimension.

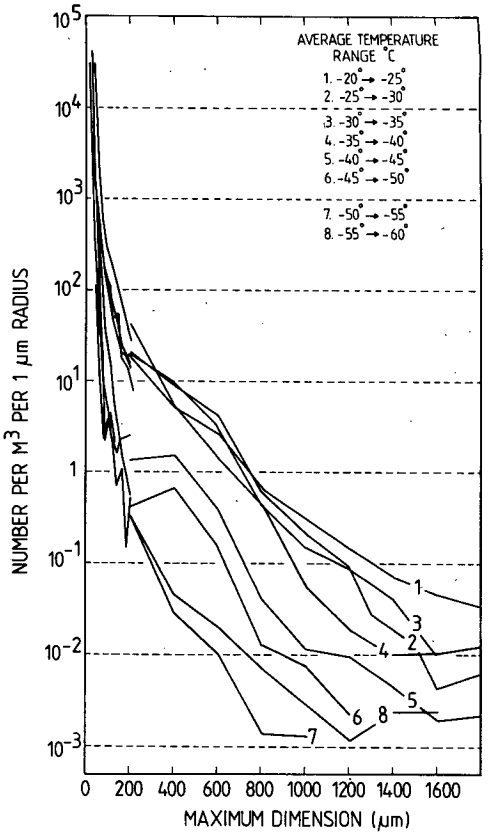

FIG. 3. As in Fig. 2, but for 20–1800 μm maximum dimension.

the *IWC* figures calculated originally by Heymsfield (1977).

Several general features of the temperature dependences of the shape of the size spectra were found. For a given particle dimension in the range 20 to 200 μm (Fig. 2), the particle concentrations remained rather similar in the temperature range −20 to −40°C, but for lower temperatures the concentrations, although again rather similar at a given dimension were considerably lower. This behavior is borne out by the values indicated in Table 2, column F, of the concentration of 100 μm particles, N_{100}. (N_{100} was estimated from curves fitted to the spectra in Figs. 2 and 3, to be discussed later.) For a given particle dimension for sizes greater than 200 μm (Fig. 3), the concentrations tended to decrease with temperature. For example, the concentration of 1000 μm particles, N_{1000}, (see Fig. 3 and also indicated in Table 2 column I) decreased by more than two orders of magnitude over the range −20 to −60°C. However, the concentration fall-off with temperature was by no means monotonic. For instance, at 600 μm (see Fig. 3), the concentrations stayed rather constant for temperatures in the −20 to −40°C range, after which they declined.

The maximum crystal dimension and the *IWC* of the averaged spectra (Table 2; columns C and D, re-

TABLE 2. Summary of cirrus particle size distribution data

	Data used in analysis				Spectra for curves averaged by temperature							Spectra for individual curves			
						Curve a			Curve b			Curve a		Curve b	
Curve number	Temperature range (°C)	Number of sampling passes	Maximum particle dimension (mm)	Range of IWC (g m^{-3})	$\overline{IWC}$* (g m^{-3})	N_{100} (m^{-3} μm^{-1})	$N_{100/\overline{IWC}}$ (g^{-1} μm^{-1})	B_1 Slope	N_{1000} (m^{-3} μm^{-1})	$N_{1000/\overline{IWC}}$ (g^{-1} μm^{-1})	B_2 Slope	$N_{100/IWC}$ (g^{-1} μm^{-1})	B_1 Slope	$N_{1000/IWC}$ (g^{-1} μm^{-1})	B_2 Slope
Column	A	B	C	D	E	F	G	H	I	J	K	L	M	N	O
1	−20 → −25	5	2.6	0.001–0.063	0.027	1.40×10^2	5.17×10^3	−2.56	0.325	12.0	−3.74	7.22×10^3 $\pm 3.97 \times 10^3$	−2.41 ± 0.21	10.60 ± 2.65	−5.02 ± 1.90
2	−25 → −30	6	1.8	0.001–0.066	0.025	1.75×10^2	7.00×10^3	−2.51	0.260	10.4	−4.49	7.70×10^3 $\pm 4.31 \times 10^3$	−2.52 ± 0.54	6.75 ± 2.80	−5.85 ± 1.55
3	−30 → −35	7	2.4	0.008–0.043	0.0175	1.30×10^2	7.43×10^3	−2.21	0.24	13.7	−3.94	8.70×10^3 $\pm 4.30 \times 10^3$	−2.27 ± 0.30	5.80 ± 4.80	−5.87 ± 1.40
4	−35 → −40	11	2.0	0.009–0.025	0.126	2.50×10^2	1.98×10^4	−2.29	0.13	10.3	−4.37	1.90×10^4 -1.78×10^4	−2.42 ± 0.42	4.46 ± 3.30	−5.46 ± 1.50
5	−40 → −45	6	1.8	0.0004–0.008	0.0034	2.55×10^1	7.50×10^3	−3.23	0.017	4.86	−3.23	8.02×10^3 $\pm 6.67 \times 10^3$	−2.87 ± 0.78	4.70 ± 3.70	−4.22 ± 1.20
6	−45 → −50	8	1.2	0.0002–0.008	0.0025	1.40×10^1	5.60×10^3	−3.15	0.010	4.00	−3.15	5.97×10^3 $\pm 1.98 \times 10^3$	−3.01 ± 0.64	2.90 ± 1.70	−3.77 ± 1.13
7	−50 → −55	4	1.6	0.0002–0.004	0.0018	7.00×10^0	3.89×10^3	−3.83	0.00155	0.86	−3.83	3.70×10^3 $\pm 4.20 \times 10^3$	−3.86 ± 0.29	6.30 ± 4.70	−3.40 ± 0.99
8	−55 → −60	4	1.0	0.0002–0.0018	0.0009	5.02×10	5.58×10^3	−3.85	0.00725	8.06	−3.85	5.70×10^3 $\pm 3.80 \times 10^3$	−3.20 ± 0.41	6.40 ± 3.90	−3.20 ± 0.41

* This is the mean ice water content for each temperature range.

spectively) generally decreased with decreasing temperature. The large decrease in *IWC* between Curves 4 and 5 is clearly evident.

Curves of exponential and power law form[3] were fitted to the data in Fig. 3 for the purpose of inferring whether a simplified means for representing the data was possible. It was found that the spectra in each temperature interval could be adequately represented by one or two curves of the form

$$N = AD^B, \tag{1}$$

where N is the number concentration (m^{-3} μm^{-1}), A the intercept parameter, B the slope, and D is the particle dimension (μm). Curves of the form of Eq. (1) are plotted for each temperature interval in Fig. 4. A single curve adequately represented the data for temperature intervals $\leq -40°C$, but two curves, one at smaller and one at larger particle sizes, referred for a given temperature interval as (a) and (b), were necessary to describe the data for temperature intervals warmer than $-40°C$; the goodness of fit of the curves was not quantified. The means by which N in Eq. (1) can be calculated for the temperature averaged spectra are discussed in Appendix B.

The curves in Fig. 4 represent the spectral forms for the averaged spectrum in each temperature interval but did not accurately represent the spectral form for each individual spectrum within a temperature interval. To examine the differences between the spectral forms of the individual and averaged spectra within each temperature interval, curves of the form given by Eq. (1) were also fitted to the individual pass-averaged size spectra. Unlike the case of the temperature-averaged spectrum, two curves, (a) and (b), were necessary to represent a spectrum for each temperature range except the lowest. The means by which N in Eq. (1) can be calculated for the individual spectra in each temperature interval is discussed in Appendix B.

Comparison of the form of the curves derived for the temperature-averaged data with that of the individual data within a temperature interval (see discussion in Appendix B) indicated the following similarities and differences:

(1) The values of B for the individual spectra in a temperature interval were nearly the same as those derived for the averaged spectrum. Along curves (a), the values corresponded closely. The values along curves (b) for the individual spectra tended to be somewhat higher than those for the temperature-averaged spectra. The above differences in the slope parameters are probably due to the presence of zero

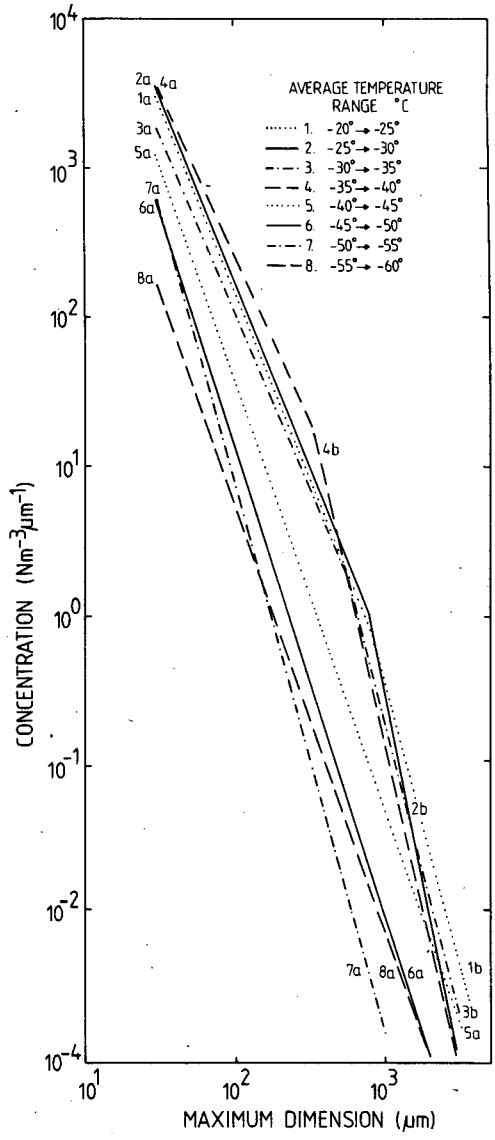

FIG. 4. Curves fitted to the average spectra for each temperature range.

counts at the larger particle sizes for individual spectra arising from the low sampling volume. These zero counts were included by averaging them with the next higher channel to obtain an average for the two combined channels. This process would tend to increase the slope B of the line.

(2) The values of A varied considerably amongst the individual spectra. However, the value of A, divided by the ice water content remained roughly the same for the individual spectra; the value of $A/\overline{IWC}$ for the corresponding temperature-averaged spectrum was also about the same. For example, at virtually all dimensions along a curve (a), the crystal concentrations divided by *IWC* for an individual spectrum were within a factor of two or three of those for the temperature-

[3] The equations were derived from curves drawn through the data by eye. It was not usually possible to use a least-squares technique for fitting the curves; channels containing zero counts would lead to obvious underestimation in the spectral slope and overestimation in the intercept if the least-squares method was used.

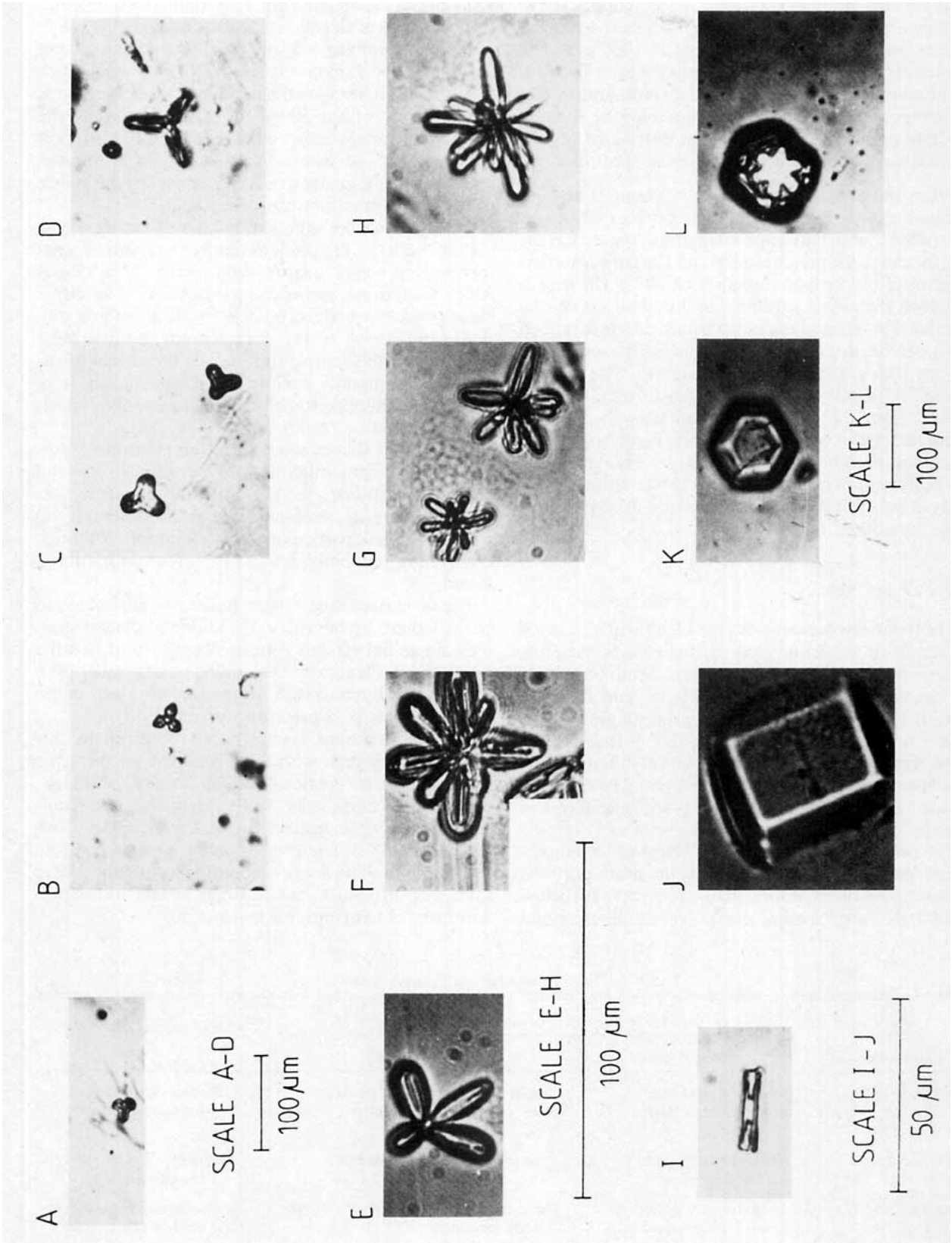

FIG. 5. Examples of replicas of ice crystals taken in cirrus during the aircraft flights. See text for details.

averaged spectra. Wider variations in the concentrations divided by the *IWC* were noted along a curve (b) between the individual and temperature-averaged spectra, particularly for dimensions > 1000 μm. The differences again are probably due to the poor statistics of the samples for the individual spectra, and in fact the temperature-averaged spectrum may be a more accurate representation of the concentrations of particles at large sizes than the individual spectra.

From the above comparisons of averaged and individual spectra in each temperature interval, it was concluded that to a first approximation, the cirrus particle spectra in the present study could be parameterized in terms of the temperature and the *IWC*. The means by which the cirrus particle size distributions can be calculated in terms of these two parameters is described in Appendix B. Of course, the normalization of the spectra with *IWC* is only approximate. The average of the *IWC*s will not be equivalent to the *IWC* calculated from the average spectra. Also, the *IWC* is calculated with certain assumptions regarding crystal shape and density. The same mixture of crystals will not be present in every individual cloud, although this study does illustrate some temperature dependence of these quantities.

b. *Ice crystal habits*

The replicator data was used to identify qualitatively the habits of the ice crystals in the clouds sampled. Examples of replicas of ice crystals obtained within the cirrus clouds are shown in Fig. 5, and the relationships noted between the ice crystal shapes and the temperature are summarized in Table 3. It should be pointed out that although a multitude of different crystal shapes were observed, most habits could be classified according to the Magono and Lee (1966) classification scheme.

The predominant crystal types observed at temperatures from −20 to −40°C within the main portions of the cirrus layers, more than about 500 m below cloud top, were "spatial" (or polycrystalline) crystal forms, including combinations of bullets (e.g., see Figs. 5a to 5d), (C2a, Magono and Lee, 1966, classification); combinations of side planes, bullets and columns (S3); radiating assemblages of plates (P7a) and side planes (S1). Hollow columnar crystals (C1f) with axial ratios > 2:1 and thin hexagonal plate-like (P1a) crystals were predominant within 500 m of cloud tops when the temperature was warmer than −40°C, and also were commonly found within the cloud layers at temperatures warmer than about −25°C. Single hollow bullets (C1d) were sometimes observed.

Ice crystal shapes sampled in the temperature range −40 to −50°C were predominantly the spatial crystal forms given above (e.g., see Figs. 5e to 5h) in clouds which contained embedded convection. For cirrus clouds which contained no discernible ascending motions, and for all of the cirrus clouds sampled near cloud top in this temperature range, the crystal forms were predominantly hollow columnar crystals (e.g., see Fig. 5i), although some hexagonal plate-like crystals were observed.

The crystal shapes sampled at temperatures below −50°C were predominantly hollow columns or solid columns (C1e) (e.g., see Fig. 5j), although some hexagonal plates (e.g., see Figs. 5k–l) or thick plates (C1g) were also noted, particularly near cloud top. Although observed infrequently, bullet rosettes were sometimes found.

For all temperature ranges, bullet rosettes tended to be the largest crystals (up to the largest measured size), with single bullets and columns being about half the rosette sizes. Planar crystals tended to be smaller than a few hundred microns. A more complete study of the replicator data is at present in progress.

The predominant crystal habits observed in this study are consistent with those reported for the same temperatures in previous studies (e.g., Weickmann, 1947; aufm Kampe *et al.*, 1951; Heymsfield and Knollenberg, 1972; Heymsfield, 1975; Varley, 1978; Conway *et al.*, 1982). The present analysis would indicate that polycrystalline forms predominate at temperatures from −20 to −40°C, while single crystal forms predominate at temperatures below −50°C.

TABLE 3. Crystal habits observed in cirrus clouds.

	Within main portions of cloud		Near cloud top
Temperature	"Convective" clouds	"Stable" clouds	
Higher than −40°C	Spatial crystal forms Some columns, plates, bullets	Spatial crystal forms Some columns, plates, bullets	Hollow columns and hexagonal plates
−40°C to −50°C	Predominantly spatial crystal forms	Predominantly hollow columns	Hollow columns and hexagonal plates
Lower than −50°C	Predominantly hollow or solid columns, some hexagonal	Predominantly hollow or solid columns, some hexagonal plates, thick hexagonal plates	Hollow or solid columns, thick hexagonal plates

TABLE 4. Comparison of particle number concentrations (m^{-3}) measured between 10 and 30 μm dimension by the FSSP and the 1D-C instruments, for arbitrarily selected sampling levels.

Flight	FSSP (10–30 μm) ($\times 10^5$)	1D-C (10–30 μm) ($\times 10^5$)
P3 Level 1	1.30	1.30
P4 Level 3	1.23	1.22
P10 Level 4	3.99	4.01
P11 Level 2	3.62	3.62
P12 Level 1	6.91	6.90

4. Cirrus extinction and backscatter

a. Estimation of the ice particle extinction

Examination of the spectral shapes of the number concentrations from the FSSP probe indicates that the parameterization described in this article would not hold in the 2–20 μm region, even assuming that the FSSP figures were correct. However, as shown in Table 4, the corresponding numbers between 10 and 30 μm measured by the FSSP and the 1D-C agree very closely. Thus the measured numbers in the 2–10 μm range may not be too far from the truth.

The optical extinction for sizes greater than 20 μm could be calculated using the parameterizations discussed here provided that some relationship between the "length" D and "diameter" U of the ice crystals can be assumed to hold. However, the contribution due to particles of sizes less than 20 μm could be appreciable. This contribution has thus been estimated using the actual data from all three probes averaged over three temperature ranges. It was assumed that the extinction coefficient was equal to twice the geometrical cross-section for all sizes and that the particles were cylindrical in shape. It was further assumed that $U = 0.057D^{0.786}$, where D is in meters (after Heymsfield, 1972) and that the radiation was incident perpendicular to the length. The results are shown in Table 5, and it is obvious that the extinction contribution from the 2–20 μm size range is very appreciable, particularly at the lower temperatures. The equivalent contribution to the infrared extinction ($\sim$10 μm) will be less because of the reduction in extinction efficiency for lengths below 10 μm. An estimate indicates that the contribution of the infrared cross-section in the 2–20 μm region will be about half that in the visible.

If the extinction in the 20 $\mu \rightarrow \infty$ size region for any IWC and temperature is calculated using the parameterized curves and some relation between length and width, an estimate of total extinction to within 10 to 20% could be obtained from the percentage figures given in Table 5.

Table 5 shows that the total extinction coefficient drops off from 1.0 km^{-1} for the $-25°C \rightarrow -40°C$ range to 0.23 km^{-1} for temperatures less than $-50°C$. This decrease is very significant for the climatic effects of cirrus. A cloud with a temperature below $-40°C$ and a depth of 1 km (see PD) will have an optical depth of 0.23—within the range of optical depths where the cirrus causes a climatic warming. The above values of the extinction coefficients agree well with values measured by lidar.

b. Lidar backscatter and cirrus particle spectra

Physical reasoning would suggest that either changes in crystal habit or particle phase would be primarily responsible for the sharp change in the lidar backscatter to extinction ratio between -35 and $-45°C$ shown in Fig. 1. What is immediately apparent from Figs. 2 and 3 is that a similar sharp change in the crystal *concentration* of the spectra occurs over the same temperature range of -35 to $-40°C$. Of course, the different shapes between the curves of Figs. 2 and 3 could well indicate a change in habit as well as concentration. In support of the former, and although the replicator results are mainly qualitative, they do point to a transition in crystal habit between predominantly spatial polycrystalline forms at temperatures greater than $-40°C$ to the more simple crystal types at lower temperatures. The change in crystal habit can also be accounted for on a physical basis by a change in the mode of ice crystal nucleation. The spatial polycrystalline forms observed at temperatures warmer than about $-40°C$ indicate that droplets greater than a few microns in size had frozen to form the initial crystals (see Magono and Aburakawa, 1968). The general lack of polycrystalline forms at temperatures below about $-40°C$ to $-50°C$ would be commensurate with laboratory findings that there is an absence of (liquid) droplets at temperatures less than $-40°C$, and thus different nucleation mechanisms (and thus crystal habits) must occur at these lower temperatures.

Information on the backscatter properties of different ice crystal habits is scarce. For complex crystalline forms (prism–planar aggregates, graupel etc.) k was found by Sassen (1978) to be 0.41, for spatial crystals, 0.26, and for small "simple" ice crystals, about 0.04. For small plates and columns ($\sim$2 to 5 μm size), k was found to be 0.1 (Sassen and Liou, 1979). Thus the "simpler" ice crystals which are found to occur in cirrus at temperatures below $-40°C$ to $-50°C$ would

TABLE 5. The percentage of the total visible extinction due to particles in the 1–20 μm size range.

Temperature range	Extinction coefficient (m^{-1}) 1–20 μm ($\times 10^{-4}$)	20 μm $\rightarrow \infty$ ($\times 10^{-4}$)	Total ($\times 10^{-4}$)	Percentage of total in 1–20 μm range
$-25°C \rightarrow -40°C$	3.58	6.64	10.22	35
$-40°C \rightarrow -50°C$	1.64	1.46	3.10	53
$< -50°C$	1.20	1.06	2.26	53

be expected to give smaller values of k than the more complex crystals found at warmer temperatures in agreement with lidar observation.

The effects of small supercooled drops should also be considered. Values of k for water drops vary in the region of 0.44 to 0.70 (Sassen and Liou, 1979; Derr, 1980). It is not clear yet whether there is a complete absence of drops (water or ice) in cirrus at temperatures below −40°C. However, an estimate of the possible maximum effect of drops on k has been obtained by assuming that for temperatures greater than −40°C, *all* particles measured by the FSSP probe, and with diameters less than 10 μm, were water droplets and that larger particles were all ice crystals. The value of k for droplets was taken as 0.7. It was assumed that *only* ice crystals existed in cirrus below −50°C. A calculation similar to that done in the last section (see Table 5) indicated that for temperatures above −40°C, 20% of the geometrical cross-section was due to particles of diameter less than 10 μm. Assuming that changes in k were due to changes in backscatter rather than extinction and that k for ice crystals was 0.25, an effective k for the above mixture of ice crystals and water drops was calculated to be 0.34. Thus, the presence of drops in cirrus could possibly influence the value of k but could not account for the total observed change in k from 0.25 to 0.45 (Fig. 1) over the observed temperature change.

5. Conclusions

The main finding of this study is that the shapes of the cirrus crystal size distributions, at least for dimensions greater than 20 μm, and the distribution of crystal habits depend to a large extent on the ambient temperature. Furthermore, the greatest changes in the particle spectra occur over a similar temperature range as the greatest changes in the cloud particle backscatter to extinction ratio as measured by lidar.

Parameterization of the particle spectra for dimensions greater than 20 μm has been achieved in terms of simple relations between particle dimension, cloud *IWC* and temperature. These curves should be very useful for parameterization of cirrus optical extinction provided that some simple relation between particle dimension and shape can be shown to be valid. It is unfortunate that the FSSP probe data were considered too unreliable because an estimate has shown that ~35% of visible extinction for temperatures greater than −40°C is due to particles with dimensions less than 20 μm, the percentage rising to over 50% at lower temperatures. The equivalent percentage of infrared extinction is less because of the decreasing infrared extinction efficiency for particles less than 10 μm.

It is clear that the 2–20 μ dimension region needs to be studied in more detail. This is being done at present on the replicator data, and spectra and particle habits will be reported later. An allied problem is the percentage of the very small particles which are spherical droplets and further study is needed on this aspect.

Qualitatively the changes in lidar-measured backscatter to extinction ratio can be related to changes in crystal habit, but the part played by supercooled drops is not clear and further measurements are needed on the backscatter and extinction properties of various ice crystal habits.

The variation in the average *IWC* values and the corresponding change in the approximate extinction coefficients is obviously significant for the influence of cirrus on climate. Clouds warmer than −40°C will tend to be more absorbing and to contain more ice than colder clouds. This is in agreement with previous lidar observations (PD).

Mass absorption coefficients for the various temperature ranges (Extinction Coefficient/$\overline{IWC}$) have not been considered here because of the uncertainty in the FSSP probe data.

Acknowledgments. Some of this work was carried out when A. J. Heymsfield was a Visiting Scientist at the CSIRO, Division of Atmospheric Research.

APPENDIX A

Problems Noted with the Data

Several problems were noted with the data from the probes on the aircraft. The primary problems are discussed in A to E below.

A) Since the forward scattering characteristics of the ice particles were unknown, it was impossible to determine the sampling volume of the FSSP probe. Thus, data from the FSSP probe were not used in the analysis herein. However, it should be pointed out that the spectra from the FSSP data which were estimated by assuming that the ice particles had scattering properties equivalent to water drops closely matched the 1D-C spectra at overlapping sizes. (Fig. 5).

B) Data from the 1D-C probe at sizes larger than 200 μm were not used in the analysis because very few particles of sizes larger than 200 μm were sampled owing to the comparatively small sampling volume of the probe at these sizes.

C) Concentrations derived from the 1D-P probe data for sizes larger than about 1 mm in each spectrum are likely to be underestimated because zero counts in certain channels, whenever they occurred, were averaged with non-zero counts to obtain a channel average. However zero counts just represented a concentration below the probe sampling volume threshold, and thus average concentrations were underestimated. Although the statistical significance of the data was questionable, the data was used because it provided an indication of the largest particle sizes that were present.

D) Underestimates in the concentration of particles measured with the 1D-P probe at dimensions from

140–420 μm were likely to have occurred when the particles at these sizes were predominately columnar in shape (see Gordon and Marwitz, 1982). Since columns predominated at temperatures below about −45°C, it is expected that the particle concentration for sizes from 140–420 μm are underestimated at these temperatures. Corrections to the spectra were already made in Heymsfield (1977) to estimate the maximum dimensions of columnar crystals.

E) Breakup of the crystals upon impact with the replicator device was not appreciable for sizes smaller than about 200 μm but was appreciable at sizes larger than about 400 μm. Although the larger crystals were often broken up, it was usually possible to identify their habits.

APPENDIX B

Calculation of the Cirrus Particle Size Distributions

The temperature-averaged and individual spectra in each temperature interval could be reasonably well represented by at most two curves[4] of the form

$$N = A_1 \times D^{B_1} \times IWC \quad \text{for} \quad D < D_0, \qquad (2)$$

$$N = A_2 \times D^{B_2} \times IWC \quad \text{for} \quad D > D_0, \qquad (3)$$

where N is the concentration (m^{-3} μm^{-1}), D the crystal maximum dimension (μm), IWC the ice water content contained by the particles over the entire spectrum, B_1 and B_2 are the slopes of the curves, and A_1 and A_2 the intercept parameter A in Eq. (1), normalized by the ice water content. Here D_0 was selected for "best-fit". Values of A_1 can be calculated from the values of the concentration at a dimension of 100 μm, N_{100} (discussed below), normalized by the IWC, from

$$A_1 = \frac{N_{100}/IWC}{(100)^{B_1}}, \qquad (4)$$

and A_2 can be obtained from the concentration at a dimension of 1000 μm, N_{1000} from

$$D_0 = \left(\frac{A_2}{A_1}\right)^{\frac{1}{B_1 - B_2}}. \qquad (5)$$

Values of the slope parameter for the curves a and b for each temperature interval of the temperature-averaged spectra are given in Table 2, columns H and K, respectively; those for the individual spectra are given in columns M and O. Values of N_{100}/IWC and N_{1000}/IWC are given for the temperature-averaged spectra in Table 2, columns G and J, respectively, and for the individual spectra in columns L and N, respectively.

[4] For temperatures < −40°C, one curve could be used to represent the data adequately. To facilitate a comparison of the data from the temperature-averaged spectra with that of the individual spectra discussed later in the appendix, coefficients are given for two curves.

As discussed in the text, the temperature-averaged size spectra represent a more statistically significant sample than the individual spectra. Thus, the form of the cirrus particle spectra should be calculated from the parameters derived from the temperature-averaged spectra in Table 2, columns G–H and J–K.

REFERENCES

aufm Kampe, H. J., H. K. Weickmann and J. J. Kelly, 1951: The influence of temperature on the shape of ice crystals growing at water saturation. *J. Meteor.*, **8**, 168–174.

Chylek, P., 1978: Extinction and liquid water content of fogs and clouds. *J. Atmos. Sci.*, **35**, 296–300.

——, and V. Ramaswamy, 1982: Simple approximation for infrared emissivity of water clouds. *J. Atmos. Sci.*, **39**, 171–177.

Conway, B. J., S. J. Caughey, A. N. Bentley and J. D. Turton, 1982: Ground-based and airborne holography of ice and water clouds. *Atmos. Environ.*, **16**, 1193–1207.

Derr, V. E., 1980: Estimation of the extinction coefficient of clouds from multiwavelength lidar backscatter measurements. *Appl. Opt.*, **19**, 2310–2314.

Gordon, G. L., and J. D. Marwitz, 1982: An airborne comparison of three PMS probes. *Proc. Conf. on Cloud Physics,* Chicago, Amer. Meteor. Soc., 267–270.

Heymsfield, A. J., 1972: Ice crystal terminal velocities. *J. Atmos. Sci.*, **29**, 1348–1357.

——, 1975: Cirrus uncinus generating cells and the evolution of cirriform clouds. Part 1. Aircraft observations of the growth of the ice phase. *J. Atmos. Sci.*, **32**, 799–808.

——, 1977: Precipitation development in stratiform ice clouds: A microphysical and dynamical study. *J. Atmos. Sci.*, **34**, 367–381.

——, and R. G. Knollenberg, 1972: Properties of cirrus generating cells. *J. Atmos. Sci.*, **29**, 1358–1366.

Magono, C., and C. V. Lee, 1966: Meteorological classification of natural snow crystals. *J. Fac. Sci.,* Hokkaido University, Ser. VII, **2**, No. 4, 321–362.

——, and H. Abarakawa, 1968: Experimental studies of snow crystals of plane type with spatial branches: *J. Fac. Sci.,* Hokkaido University, Ser. VII, **3**, 85–97.

Paltridge, G. W., 1974: Infrared emissivity, shortwave albedo and the microphysics of stratiform water clouds. *J. Geophys. Res.*, **79**, 4053–4058.

Platt, C. M. R., 1976: Infrared absorption and liquid water content in stratocumulus cloud. *Quart. J. Roy. Meteor. Soc.*, **102**, 533–561.

——, 1981: The effect of cirrus of varying optical depth on the extraterrestrial net radiative flux. *Quart. J. Roy. Meteor. Soc.*, **107**, 671–678.

——, and A. C. Dilley, 1981: Remote sounding of high clouds. IV: Observed temperature variations in cirrus optical properties. *J. Atmos. Sci.*, **38**, 1069–1082.

Sassen, K., 1978: Backscattering cross sections for hydrometeors: Measurements at 6328 Å. *Appl. Opt.*, **17**, 804–806.

——, and K. N. Liou, 1979: Scattering of polarized laser light by water droplet, mixed-phase and ice crystal clouds. Part II: Angular depolarizing and multiple-scattering behavior. *J. Atmos. Sci.*, **36**, 852–861.

Stephens, G. L., 1978: Radiation profiles in extended water clouds. II: Parameterization schemes. *J. Atmos. Sci.*, **35**, 2123–2132.

——, and P. J. Webster, 1981: Clouds and climate: Sensitivity of simple systems. *J. Atmos. Sci.*, **38**, 235–247.

Varley, D. J., 1978: Cirrus particle distribution study, Part 3. No. AFGL-IR-78-0305, *Air Force Surveys in Geophysics,* No. 404. Air Force Geophysics Laboratory, Hanscom AFB, MA, 67 pp.

Weickmann, H., 1947: *Die Eisphase in der Atmosphare.* Library Trans. 273, Royal Aircraft Establishment, Farnborough, 96 pp.